J. Fluid Mech. (1996), *vol.* 313, *pp.* 343–366

On laminar free convection in inclined rectangular enclosures

By LARS-GÖRAN SUNDSTRÖM[1] AND SHIGEO KIMURA[2]†

[1]Department of Mechanics, Royal Institute of Technology, S-100 44 Stockholm, Sweden

[2]Tohoku National Industrial Research Institute, Sendai, Japan

(Received 19 January 1995 and in revised form 25 July 1995)

A class of problems of natural convection in tilted boxes is studied by analytical and numerical methods. The convection is assumed to be driven by uniform fluxes of heat (or mass) at two opposing walls, the remaining walls being perfect insulators. Disregarding end-region effects, an exact analytical solution is derived for the state which occurs after initial transients have decayed. This state is steady except for a spatially uniform, linear growth in the temperature (or the species concentration) which occurs whenever the fluxes are not equal. It is characterized by a uni-directional flow, a linear stratification and wall-to-wall temperature profiles which, except for the difference in absolute values due to the stratification, are the same at each cross-section. The mathematical problem is in essence nonlinear and multiple solutions are found in some parameter regions. The Bénard limit of horizontal orientation and heating from below is found to give a first bifurcation for which the steady states both before and after the bifurcation are obtained analytically. For a tilted Bénard-type problem, a steady state with top-heavy stratification is found to exist and compete with a more natural solution. The analytical solution is verified using numerical simulations and a known approximate solution for a vertical enclosure at high Rayleigh numbers. The presented solution admits arbitrary Rayleigh numbers, inclination angles and heat fluxes. Some restrictions on its validity are discussed in the paper.

1. Introduction

Natural convection in enclosures is and has long been a subject of intense research. It occurs in everyday life, for instance in double-glazed windows and car batteries, as well as in industrial processes such as crystal growth and electrochemical metal refining. The density differences which, when acted upon by gravity, cause the convection are generally due to differences in either temperature or chemical composition (or both).

In the following very limited review of the literature, we will focus on rectangular enclosures where the flow is driven by either prescribed heat/mass fluxes or prescribed temperatures/concentrations at two opposing sides. Unless otherwise stated, two-dimensional geometries are considered.

One much studied case, generally referred to as Rayleigh–Bénard convection, is that of a horizontal enclosure with its lower wall maintained at a higher temperature than its upper. For this case a solution without convection exists, but it is only stable for low Rayleigh numbers. Assuming infinite length and depth, the critical Rayleigh number based on the height becomes 1708. At this value, convection starts

† Present address: Department of Mechanical Engineering, Kanazawa University, Kodatsuno 2-40-20, Kanazawa 920, Japan.

in the form of horizontal rolls. If the heat flux, rather than the temperature itself, is prescribed at the boundaries, the critical Rayleigh number goes down to 720, as shown by Sparrow, Goldstein & Jonsson (1963) who obtained stability results for a variety of boundary conditions.

Taking all the four sidewalls into account, Davis (1967) shows that smaller length and depth of the box gives a higher critical Rayleigh number and that the rolls orient themselves with their axes of rotation parallel to the shorter of the two dimensions.

On increasing the Rayleigh number, a complex scenario of Prandtl-number-dependent transitions occurs before the flow eventually becomes turbulent. The review by Busse (1978) gives detailed information about this, whereas the work by Stella, Guj & Leonardi (1993) can serve as an introduction to more recent work. An extensive review of the research on Rayleigh–Bénard convection as a whole can be found in Drazin & Reid (1981, chap. 2).

Another fundamental case is that of a vertical enclosure with its sidewalls maintained at different temperatures. A theoretical treatment of this case was first done by Batchelor (1954), who made a perturbation series solution for the conduction-dominated regime. A heat transfer estimate for the convection-dominated regime was also arrived at, assuming an isothermal interior. However, when experimental data became available they gave contrary evidence of a stratified inner region.

Elder (1965) made extensive measurements of temperature and velocity in a tall box, again with differential heating. He also presented an analytical solution, originally due to Prandtl (1952) in his model for the wind due to a warm mountain slope, based on the assumption of uni-directional flow and therefore valid only near mid-height, as explained by him. The solution contains a linear stratification constant, which could not be determined in a straightforward way.

Subsequently, Gill (1966) extended Elder's solution to take the varying boundary-layer thickness into account. However, Gill's solution also has a constant whose determination has been questioned in later works. For determining the constant in Gill's solution, Bejan (1979) used the approximate argument that there should be no net energy transport in horizontal cross-sections near the ends.

For the case of constant heat flux, treated by Kimura & Bejan (1984), the above argument becomes applicable at arbitrary cross-sections and, when applied to Elder's original solution, actually gives an exact solution of the boundary-layer equations in the interior. The solution thus obtained was verified using a numerical simulation.

Since it takes a long time to reach the steady state, time-dependent problems are also of great practical interest. Scaling arguments and numerical simulations by Patterson & Imberger (1980) suggest that for high Rayleigh numbers the steady state is approached via damped internal waves. In a numerical simulation Schladow (1990) detected both the internal waves and two other types of oscillatory motion which were found to be due to two different types of boundary-layer instabilities. In both the above studies, constant wall temperatures were prescribed – although the choice of boundary conditions appears not to be crucial for the phenomena as such.

Recently, Bark, Alavyoon, & Dahlkild (1992) extended the solution of Kimura & Bejan (1984) to encompass the case of constant fluxes which are not equal. Such situations occur frequently in electrochemical systems such as lead-acid batteries. In the same paper an equation for the development of stratification with time was developed. Bark *et al.* confirmed their findings using numerical and experimental data.

Turning our attention to tilted enclosures, Hart (1971) made a linear stability analysis of the flow in an inclined box with constant-temperature boundary conditions. Stream- and spanwise perturbations were separately considered and added to a

parallel flow solution similar to that of Elder (1965), which had been extended by abandoning the boundary-layer assumption. Both the analysis and experiments presented in Hart (1971) show the existence of two different instability mechanisms, effective in different parameter regions: longitudinal rolls and transverse travelling waves. The analytical results were in fair agreement with the experiments considering that the base solution used did not fulfil the constant-temperature boundary conditions imposed in the experiment – an approximation that Hart was well aware of. Had it not been for the zero temperature fluctuation which was imposed on the perturbations and the fitting of the stratification to experimental data, Hart's results would have been directly applicable to the present analysis.

An analysis which is very similar to the one to be presented here is that of Sen, Vasseur & Robillard (1987), who considered an inclined porous layer with a prescribed heat flux through it (no heat accumulation). We shall have reason to return to their work during the course of our analysis.

In the following, we will treat the case of an inclined tall enclosure with constant, generally different, heat fluxes prescribed at the two sidewalls. Both arbitrary Rayleigh numbers and an arbitrary angle of inclination will be allowed for. In spite of its rather fundamental nature this problem appears not to have been considered before. We will look for a solution using a simple ansatz with a linear stratification. Working with real variables, we get two different families of solutions depending on the sign of the stratification. The stratification is finally determined using the energy argument of Bejan (1979), whose correctness we ascertain by deriving it from the equations and boundary conditions. We obtain a transcendental equation for the stratification which we solve numerically. Some approximate explicit solutions are also derived for the limits of low and high Rayleigh numbers. For the special case of horizontal orientation the original ansatz breaks down – however the problem becomes simpler and an explicit solution is found. A few numerical results are also presented, mainly to check the correctness of the analytical solution.

2. Problem formulation

In the following, the two problems depicted in figures 1 (*a*) and (*b*) will be treated simultaneously. Problem (*a*) is one of heat transfer whereas problem (*b*) is an electrochemical problem concerned with mass transfer in a binary electrolyte, i.e. one that contains two different ion species, one positive and the other negative. Even though the transport of ion species inside an electrolyte is not only diffusive-convective but also has the additional transport mechanism of migration due to an electric field, there is a condition of electroneutrality which can be used to write the two concentration equations for the two different species as one single equation having the same form as if the transport occurred solely by diffusion and convection (Newman 1991). To map the two problems onto one and at the same time get rid of unnecessary parameters, the following non-dimensional variables are introduced:
for the heat transfer case

$$t = \frac{t^* k}{\rho c_p h^2}, \quad x = \frac{x^*}{h}, \quad y = \frac{y^*}{h}, \quad \theta = \frac{T - T_0}{\Delta_T h}, \quad \boldsymbol{u} = \frac{\nu \boldsymbol{u}^*}{\beta_T \Delta_T h^3 g}, \quad p = \frac{p^*}{\beta_T \Delta_T \rho h^2 g}, \tag{2.1a–f}$$

$$Ra = \frac{\beta_T \Delta_T h^4 g \rho c_p}{\nu k}, \quad Pr = \frac{\nu \rho c_p}{k}, \quad A = \frac{H}{h}, \quad \lambda_1 = \frac{\Delta_{1T}}{\Delta_T}, \quad \lambda_2 = \frac{\Delta_{2T}}{\Delta_T}, \tag{2.1g–k}$$

where

$$\Delta_T = (\Delta_{1T}^2 + \Delta_{2T}^2)^{1/2}; \tag{2.1l}$$

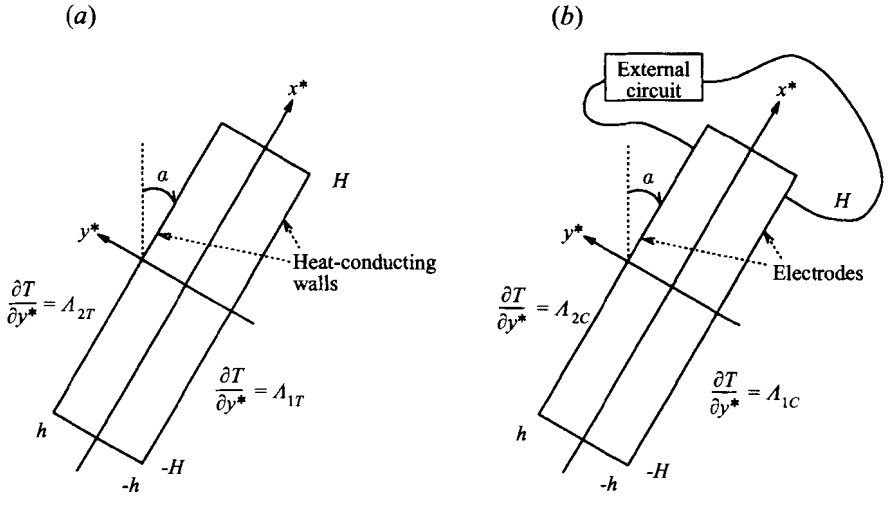

FIGURE 1. Geometry and coordinate system.

for the mass transfer case:

$$t = \frac{t^* D}{h^2}, \quad x = \frac{x^*}{h}, \quad y = \frac{y^*}{h}, \quad \theta = \frac{C_0 - C}{\Lambda_C h}, \quad \boldsymbol{u} = \frac{\nu \boldsymbol{u}^*}{\beta_C \Lambda_C h^3 g}, \quad p = \frac{p^*}{\beta_C \Lambda_C \rho h^2 g}, \tag{2.2a–f}$$

$$Ra = \frac{\beta_C \Lambda_C h^4 g}{\nu D}, \quad Pr = \frac{\nu}{D}, \quad A = \frac{H}{h}, \quad \lambda_1 = -\frac{\Lambda_{1C}}{\Lambda_C}, \quad \lambda_2 = -\frac{\Lambda_{2C}}{\Lambda_C}, \tag{2.2g–k}$$

where

$$\Lambda_C = (\Lambda_{1C}^2 + \Lambda_{2C}^2)^{1/2}. \tag{2.2l}$$

Here, β_T and β_C are volumetric expansion coefficients (in $m^3\ K^{-1}$ and $m^3\ mol^{-1}$, respectively). The remaining quantities appearing in the right-hand sides, which are not explained by figure 1, are in a standard notation. To get the same notation for both problems we have used Pr rather than Sc for the Schmidt number in the mass transfer case. Note also the sign shift in the definition of θ.

Using the Boussinesq assumption and also assuming constant material properties the non-dimensional system of equations for the quantities defined above is

$$\frac{1}{Pr}\left(\frac{\partial \boldsymbol{u}}{\partial t} + Ra(\boldsymbol{u}\cdot\nabla)\boldsymbol{u}\right) = -\nabla p + \nabla^2 \boldsymbol{u} - \theta \boldsymbol{e}_g, \tag{2.3}$$

$$\nabla \cdot \boldsymbol{u} = 0, \tag{2.4}$$

$$\frac{\partial \theta}{\partial t} + Ra\,\boldsymbol{u}\cdot\nabla\theta = \nabla^2\theta, \tag{2.5}$$

$$\text{at } y = -1: \qquad \boldsymbol{u} = 0, \qquad \frac{\partial \theta}{\partial y} = \lambda_1; \tag{2.6a,b}$$

$$\text{at } y = +1: \qquad \boldsymbol{u} = 0, \qquad \frac{\partial \theta}{\partial y} = \lambda_2; \tag{2.7a,b}$$

$$\text{at } x = \pm A: \qquad \boldsymbol{u} = 0, \qquad \frac{\partial \theta}{\partial x} = 0. \tag{2.8a,b}$$

Whenever desired, the two fluxes can be described using only one parameter γ:

$$\lambda_1 = \cos\gamma, \qquad \lambda_2 = \sin\gamma. \tag{2.9a,b}$$

The direction of gravity $\boldsymbol{e}_g = (-\cos\alpha, -\sin\alpha)$. The full problem thus has five different non-dimensional parameters: the Rayleigh number Ra, the Prandtl number Pr, the aspect ratio A, the inclination angle α, and the heating parameter γ.

3. Solution procedure

3.1. *Ansatz*

From the semi-infinite heated-slope problem treated by Prandtl (1952) we have seen how a linearly stratified temperature field far from a wall, together with suitable boundary conditions on the wall, can cause a structure with non-developing boundary layers. For a flow confined between two parallel walls, the same balance in the equations gives exact solutions with parallel flow (Hart 1971). That this works even for low Rayleigh numbers is noteworthy (but perhaps not so surprising). Instead of prescribing the stratification, as those authors did, one can prescribe the heat flux on the walls and calculate the stratification, as was done by Kimura & Bejan (1984). With non-equal heat fluxes Bark *et al.* (1992) found essentially the same structure, only with the addition of a spatially uniform, time-linear growth in temperature. It is thus with some confidence that we can make the following ansatz in searching for a solution valid for large times sufficiently far from the ends $x = \pm A$:

$$\boldsymbol{u} = u(y)\,\boldsymbol{e}_x, \tag{3.1}$$

$$\theta = f(y) + \Gamma\, t + S\,\xi, \text{ where } \xi = x\cos\alpha + y\sin\alpha, \tag{3.2}$$

$$p = P(x,y) + \Gamma\, t\,\xi + \tfrac{1}{2}S\,\xi^2. \tag{3.3}$$

Naturally, this ansatz does not (and need not) satisfy the boundary conditions at $x = \pm A$. We will continue under the tacit assumption that matching end-region solutions exist, and refer the reader to the Appendix for an example of such a solution and a general discussion of the end regions.

Inserting the ansatz into the equations one easily shows that the reduced pressure P must have a constant gradient in the x-direction. Defining $G = \partial P/\partial x$ we obtain the following ordinary differential equations:

$$\frac{\mathrm{d}^2 u}{\mathrm{d}y^2} + f\cos\alpha = G, \tag{3.4}$$

$$\frac{\mathrm{d}^2 f}{\mathrm{d}y^2} - Ra\,S\,u\cos\alpha = \Gamma, \tag{3.5}$$

with the boundary conditions

$$u(\pm 1) = 0, \qquad \frac{\mathrm{d}f}{\mathrm{d}y}(-1) = \lambda_1 - S\sin\alpha, \qquad \frac{\mathrm{d}f}{\mathrm{d}y}(1) = \lambda_2 - S\sin\alpha. \tag{3.6a–c}$$

Had we instead followed Sen *et al.* (1987) in defining the stratification S as the derivative of the temperature in the x-direction, there would have been no stratification term in the boundary conditions. Instead, an additional term would have appeared in (3.4) since it would no longer have been possible to write the buoyancy due to S as a gradient and include it in the pressure. It turns out that the solutions which have boundary-layer character also have an interior which is linearly stratified in

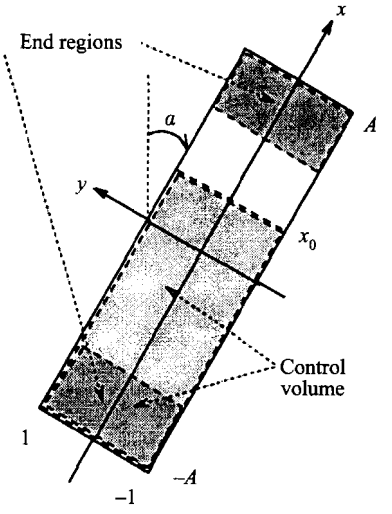

FIGURE 2. Control volume used in deriving integral conditions.

the direction of gravity, which supports our definition. Close to the bottom-heated, horizontal case, however, the physics of the problem is entirely different and the definition of Sen *et al.* works better in that as $\alpha \to \pi/2$ their stratification parameter remains finite, whereas our S goes to infinity (with $S\cos\alpha$ remaining finite).

3.2. *Closing the problem*

Because of the unknown constants G, Γ, and S the system is still not closed. We will now make indirect use of the boundary conditions at the end regions to determine all the constants. First, we integrate the mass continuity equation across the control volume in figure 2 and use Gauss' theorem to write the result as a line integral around the boundary:

$$0 = \int_{-1}^{1}\int_{-A}^{x_0} \nabla\cdot\boldsymbol{u}\ \mathrm{d}x\,\mathrm{d}y = \oint \boldsymbol{u}\cdot\boldsymbol{n}\,\mathrm{d}s = \int_{-1}^{1} u\,\mathrm{d}y. \tag{3.7}$$

Even though one could have guessed this result right away, it seems that the technique used provides a formally correct way to literally go around the difficult region and obtain useful information. Integrating (3.5) from -1 to 1, the above condition on u directly gives

$$\Gamma = \frac{\lambda_2 - \lambda_1}{2}. \tag{3.8}$$

Next, we derive the energy flux condition of Bejan (1979) by proceeding in the same manner with the temperature equation:

$$0 = \int_{-1}^{1}\int_{-A}^{x_0} \frac{\partial\theta}{\partial t} + \nabla\cdot(Ra\boldsymbol{u}\,\theta - \nabla\theta)\ \mathrm{d}x\,\mathrm{d}y = \int_{-1}^{1}\int_{-A}^{x_0} \frac{\partial\theta}{\partial t}\ \mathrm{d}x\,\mathrm{d}y + \oint (Ra\boldsymbol{u}\,\theta - \nabla\theta)\cdot\boldsymbol{n}\,\mathrm{d}s. \tag{3.9}$$

With Γ as above this simplifies to

$$\int_{-1}^{1}\left(Rau\theta - \frac{\partial\theta}{\partial x}\right)\mathrm{d}y = 0, \tag{3.10}$$

which is equivalent to the condition suggested by Bejan and which, once everything else is known, will determine the stratification, S. For less idealized boundary conditions, in which the local heat flux depends on the local temperature, (3.10) would be modified to also contain an integral in x over the difference in wall heat flux $[\partial\theta/\partial y]_{y=-1}^{y=1}$ and an integral in y over the heat flux through the end surface at $x = -A$.

Letting $x_0 = A$ in (3.9) we also obtain the mean temperature in the box as a function of time: $\theta_{mean} = t(\lambda_2 - \lambda_1)/2$, which is valid even for small times when the asymptotic behaviour has not yet been approached. Combining this with the ansatz gives the following condition on f:

$$\int_{-1}^{1} f \, dy = 0, \tag{3.11}$$

from which, at a later stage, G can be determined. The solutions for f and u depend on whether S is positive or negative. One common feature of the two cases is that if f and u are split into odd and even parts, the solutions take the following form:

$$f = f_O + f_E = F_O\left(\frac{\lambda_1+\lambda_2}{2} - S\sin\alpha\right) + F_E\left(\frac{\lambda_2-\lambda_1}{2}\right), \tag{3.12}$$

$$u = u_O + u_E = U_O\left(\frac{\lambda_1+\lambda_2}{2} - S\sin\alpha\right)\cos\alpha + U_E\left(\frac{\lambda_2-\lambda_1}{2}\right)\cos\alpha, \tag{3.13}$$

where the functions F_O, F_E, U_O, and U_E depend only on y and the parameter combination $RaS\cos^2\alpha$. Using this partition, the equation for determining S can be written

$$\left(\frac{\lambda_1+\lambda_2}{2} - S\sin\alpha\right)^2 I_1 + S\sin\alpha\left(\frac{\lambda_1+\lambda_2}{2} - S\sin\alpha\right) I_2 + \left(\frac{\lambda_2-\lambda_1}{2}\right)^2 I_3 - \frac{2S}{Ra} = 0, \tag{3.14a}$$

where

$$(I_1, I_2, I_3) = \left(\int_{-1}^{1} U_O F_O \, dy, \int_{-1}^{1} U_O y \, dy, \int_{-1}^{1} U_E F_E \, dy\right). \tag{3.14b}$$

We note that the aspect ratio, A, does not enter the problem (other than in the bounds for the x-coordinate). This is a fortunate side-effect of the assumption of uniform heat/mass fluxes which, from the discussion following (3.10), is not to be expected for cases with non-uniform fluxes.

Finally, it should be noted that, even though (3.4) and (3.5) can be solved as a linear system in u and f, we are still solving a nonlinear problem because S depends on u and f. This means that there is no guarantee that there is a unique solution and indeed we shall see that there are cases with multiple solutions.

3.3. *Solution for a fixed positive S (natural stratification)*

Define

$$\beta = \left(\frac{RaS\cos^2\alpha}{4}\right)^{1/4} \qquad \text{(the positive real root only)}, \tag{3.15}$$

$$a = \tan\beta + \tanh\beta, \quad b = \tan\beta - \tanh\beta, \quad c = \cot\beta + \coth\beta, \quad d = \cot\beta - \coth\beta, \tag{3.16a–d}$$

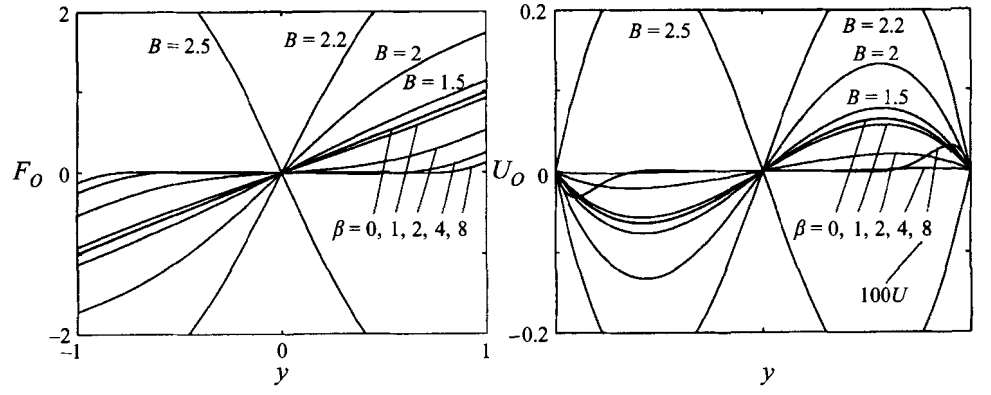

FIGURE 3. The functions $F_O(y)$ and $U_O(y)$.

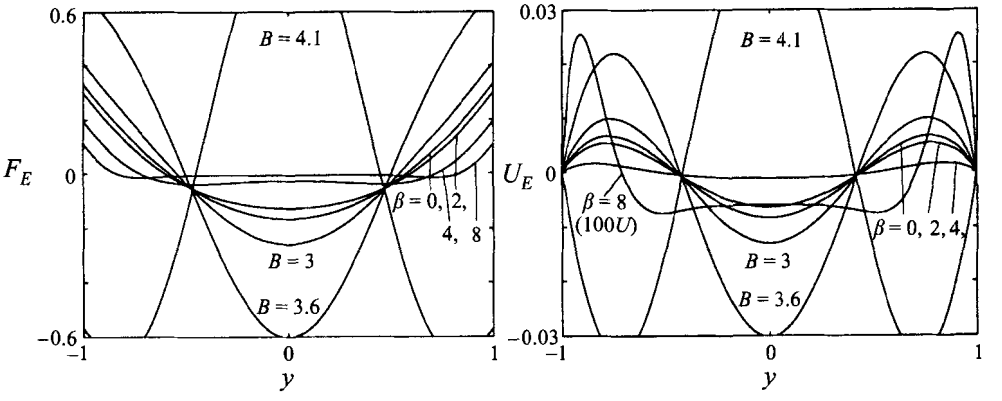

FIGURE 4. The functions $F_E(y)$ and $U_E(y)$.

then

$$F_O = \frac{1}{\beta(b+c)}\left\{\frac{\sinh\beta y\cos\beta y}{\cosh\beta\sin\beta} + \frac{\cosh\beta y\sin\beta y}{\sinh\beta\cos\beta}\right\}, \tag{3.17}$$

$$U_O = \frac{1}{2\beta^3(b+c)}\left\{\frac{\sinh\beta y\cos\beta y}{\sinh\beta\cos\beta} - \frac{\cosh\beta y\sin\beta y}{\cosh\beta\sin\beta}\right\}, \tag{3.18}$$

$$F_E = \frac{1}{2\beta^2}\left\{\frac{\sinh\beta y\sin\beta y}{\cosh\beta\cos\beta}\frac{d+2\beta}{a+d} - \frac{\cosh\beta y\cos\beta y}{\sinh\beta\sin\beta}\frac{a-2\beta}{a+d} + \frac{ac-bd-2\beta(b+c)}{2\beta(a+d)}\right\}, \tag{3.19}$$

$$U_E = \frac{1}{4\beta^4}\left\{\frac{\cosh\beta y\cos\beta y}{\cosh\beta\cos\beta}\frac{d+2\beta}{a+d} + \frac{\sinh\beta y\sin\beta y}{\sinh\beta\sin\beta}\frac{a-2\beta}{a+d} - 1\right\}. \tag{3.20}$$

(The odd functions F_O and U_O for $S > 0$ previously appeared in the work by Hart (1971).) Figures 3 and 4 show the behaviour of these four functions for some different values of β. For β smaller than about 1 (even) or 0.5 (odd) all curves lie on top of each other having no β dependence. When β is increased beyond 1 the curves rapidly move away from the small-β limit and acquire more of a boundary-layer character, the boundary-layer thickness being of the order of magnitude $1/\beta$.

Amplitudes are found to decrease as β increases. The curves marked $B = \ldots$ are related to the solution for negative S.

The integrals in the expression for determining S become

$$I_1 = \frac{1}{2\beta^4(b+c)}\left\{\frac{ac-bd}{8\beta} - \frac{2}{\sinh 2\beta + \sin 2\beta}\right\}, \tag{3.21}$$

$$I_2 = \frac{1}{2\beta^4}\left\{1 - \frac{ac-bd}{2\beta(b+c)}\right\}, \tag{3.22}$$

$$I_3 = \frac{1}{8\beta^6}\left\{\frac{ac-bd-2\beta(b+c)}{\beta(a+d)} - \frac{(a-2\beta)(d+2\beta)(4\beta+\sinh 2\beta\cos 2\beta+\cosh 2\beta\sin 2\beta)}{\beta(a+d)^2\sinh 2\beta\sin 2\beta}\right.$$
$$\left. + \left(\frac{(a-2\beta)^2}{\sinh^2\beta\sin^2\beta} - \frac{(d+2\beta)^2}{\cosh^2\beta\cos^2\beta}\right)\frac{\sinh 2\beta\cos 2\beta - \cosh 2\beta\sin 2\beta}{8\beta(a+d)^2}\right\} \tag{3.23}$$

3.4. *Solution for a fixed negative S (unnatural stratification)*

Define

$$B = \left(-Ra\,S\cos^2\alpha\right)^{1/4} \qquad \text{(the positive real root only)}, \tag{3.24}$$

$$p = \tan B, \quad q = \tanh B, \quad r = \cot B, \quad s = \coth B, \tag{3.25a–d}$$

then

$$F_O = \frac{1}{B(r+s)}\left\{\frac{\sin By}{\sin B} + \frac{\sinh By}{\sinh B}\right\}, \tag{3.26}$$

$$U_O = \frac{1}{B^3(r+s)}\left\{\frac{\sin By}{\sin B} - \frac{\sinh By}{\sinh B}\right\}, \tag{3.27}$$

$$F_E = \frac{1}{B^2(p-q)}\left\{\frac{\cos By}{\cos B}(q-B) + \frac{\cosh By}{\cosh B}(p-B) - \frac{2p\,q}{B} + p + q\right\}, \tag{3.28}$$

$$U_E = \frac{1}{B^4(p-q)}\left\{\frac{\cos By}{\cos B}(q-B) - \frac{\cosh By}{\cosh B}(p-B) + p - q\right\}. \tag{3.29}$$

Although these functions may seem a bit simpler than the ones for the naturally stratified case, their behaviour turns out to be more complex. Figures 3 and 4 indicate that for small B the curves approach the same limiting curves as for the case of positive S and $\beta \to 0$. As B is increased, the curves move away from the small-B limit, now in the opposite direction from the case of positive S. At $B \approx 2.365$ for the odd functions and $B \approx 3.927$ for the even ones a singularity occurs. Passing the singularity the curves flip over at infinite amplitude. As B is increased further, new singularities occur, but to keep the graphs readable we have chosen not to include these. Between the singular points the amplitude decreases with B. In contrast to the case of stable stratification, boundary layers do not develop. Instead, the curves become more and more wavy, their wavenumber being of order B. The singularities are found to occur at $\tanh B = -\tan B$ and at $\tanh B = \tan B$ for the odd and even functions respectively.

The integrals in the expression for determining S become

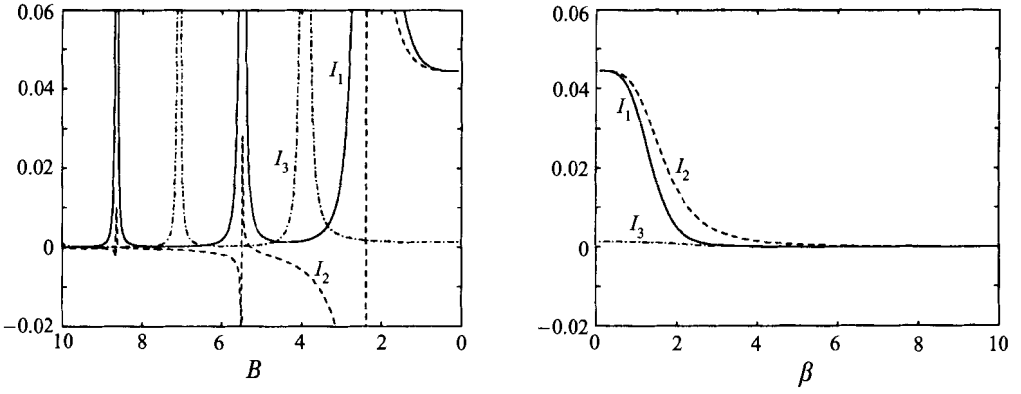

FIGURE 5. The functions I_1, I_2 and I_3 appearing in the equation for S.

$$I_1 = \frac{1}{B^4(r+s)^2}\left\{\frac{2B-\sin 2B}{2B\sin^2 B}+\frac{2B-\sinh 2B}{2B\sinh^2 B}\right\}, \tag{3.30}$$

$$I_2 = \frac{2}{B^4(r+s)}\left\{\frac{2}{B}-(r+s)\right\}, \tag{3.31}$$

$$I_3 = \frac{2}{B^6(p-q)^2}\left\{\frac{(q-B)^2(2B+\sin 2B)}{4B\cos^2 B}-\frac{(p-B)^2(2B+\sinh 2B)}{4B\cosh^2 B} +(p-q)\left(\frac{2pq}{B}-p-q\right)\right\}. \tag{3.32}$$

3.5. *Determination of S*

For the general case, it is not possible to obtain a closed form expression for S, owing to the algebraic complexity of (3.14). Studying the functions I_1, I_2, and I_3, which appear in (3.14) and are plotted in figure 5, we shall first make some observations concerning the existence of solutions before we eventually solve (3.14) numerically. For negative S all the I have singular points and the only conclusion that comes easily is that for the special case $\alpha = 0$ there are no negative solutions. For positive S, however, all the I are positive and well behaved and a more general conclusion can be drawn. Expressing S in terms of β and studying the limits $\beta \to 0$ and $\beta \to \infty$ we can show that, for all α, γ, and Ra, the left-hand side of (3.14) starts at 1/45 and goes to a negative number proportional to $-\beta^4$ as β goes from zero to infinity. Since all the functions involved are continuous, there must be at least one positive solution S to equation (3.14). In fact, in our numerical solutions of (3.14) exactly one positive solution was found for all parameter combinations tested.

We have so far allowed for arbitrary values of α and γ. However, because a number of symmetries are present we need to solve S only for the parameter ranges $0 \leqslant \alpha \leqslant 90°$ and $45° \leqslant \gamma \leqslant 225°$. The following symmetries of the unknown function $S(Ra, \alpha, \gamma)$ can then be used:

$$S(Ra, \alpha + n \times 360°, \gamma + m \times 360°) = S(Ra, \alpha, \gamma), \qquad m, n \text{ integers}, \tag{3.33}$$

$$S(Ra, 180° - \alpha, \gamma) = S(Ra, \alpha, \gamma), \tag{3.34}$$

$$S(Ra, -\alpha, \gamma) = S(Ra, \alpha, \gamma + 180°), \tag{3.35}$$

$$S(Ra, \alpha - 180°, \gamma) = S(Ra, \alpha, \gamma + 180°), \tag{3.36}$$

$$S(Ra, \alpha, \gamma = 45° + \phi) = S(Ra, \alpha, \gamma = 45° - \phi), \qquad \phi \text{ real}. \tag{3.37}$$

The symmetries (3.33)–(3.36) are purely geometric and as such quite trivial: they just describe different ways of specifying the same physical situation. On the other hand, the last symmetry (3.37), which can be shown from inspection of (3.14), does have a physical implication. It means that, as far as the solution of S is concerned, the fluxes λ_1 and λ_2 are interchangeable. For instance, supplying a certain amount of heat at the topmost boundary gives the same stratification as removing the same amount of heat at the lower boundary.

To obtain curves $S(Ra)$ for different values of α and γ, assuming no *a priori* knowledge of the number of roots, we have solved S graphically by repeatedly plotting the contour for the left-hand side of (3.14)= 0 in the (S, Ra)-plane. Whenever more accurate solutions were needed, they were found using the van Wijngaarden–Dekker–Brent method (Brent 1973), implemented in Press *et al.* (1986).

3.6. *Explicit solution for the case of horizontal orientation*

When $\alpha = \pi/2$, the original ansatz breaks down because it no longer allows θ to depend on x. As $\alpha \to \pi/2$, our numerical solutions of the stratification equation indicate that, for bottom heating ($\lambda_1 + \lambda_2 < 0$), S goes to infinity in such a way that $S\cos\alpha$ remains finite. The term $S\sin\alpha$ then goes to infinity, but cancels with a corresponding part in the function $f(y)$. This leads us to an alternative ansatz with a linear stratification S_x in the x-direction rather than in the direction of gravity. The case becomes quite simple, because the buoyancy term vanishes, and the complete solution is found to be:†

$$\theta = \frac{\lambda_2 - \lambda_1}{2} t + S_x x + \frac{Ra S_x^2}{6}\left(\frac{y^5}{20} - \frac{y^3}{6} + \frac{y}{4}\right) + \frac{\lambda_2 - \lambda_1}{2}\left(\frac{y^2}{2} - \frac{1}{6}\right) + \frac{\lambda_2 + \lambda_1}{2} y, \quad (3.38)$$

$$u = \frac{S_x}{6}(y^3 - y). \quad (3.39)$$

The condition (3.9) still holds and, with the above expressions inserted, gives a third-order polynomial equation for S_x which is easy to solve because an S_x can be factored out. Thus, $S_x = 0$ is always one solution, corresponding to pure conduction. For $\lambda_1 + \lambda_2 < 0$ and $Ra > -90/(\lambda_1 + \lambda_2)$ there are also two other solutions:

$$S_x = \pm\frac{3}{2Ra}[-7(90 + Ra(\lambda_2 + \lambda_1))]^{1/2} \quad (3.40)$$

From an intuitive comparison with the buckling beam problem one would expect that these two solutions are both stable, whereas the $S_x = 0$ solution is only stable when the other two do not exist. This is also what is indicated by numerical simulations that we have made with a two-dimensional code. For a porous medium Sen *et al.* (1987) found the same type of branching, also did two-dimensional simulations and drew the same conclusions about stability of the different branches. However, as Ra is increased further from the first bifurcation point we would expect secondary instabilities to occur. For the porous medium it was found by Kimura, Vynnycky & Alavyoon (1995) that a three-dimensional secondary instability normally sets in at a *lower* Ra than that of a competing two-dimensional instability. Naturally a three-dimensional instability, if present, would not be captured in our simulations.

Finally, we note that when our Ra is converted to a Rayleigh number based on $2h$

† The important special case $\lambda_1 = \lambda_2$ has been solved independently by Dr F. Alavyoon.

and A_1 its critical value becomes 720 for the case of equal fluxes, in perfect agreement with the stability analysis of Sparrow *et al.* (1963).

4. Numerical solution method

In order to ascertain the correctness of the analytical solution presented a few numerical simulations were made. These simulations solved the unsteady two-dimensional problem in the creeping flow approximation, i.e. neglecting the left-hand side of the momentum equation (2.3), starting from rest. A slightly modified version of a Fortran code originally written for a double-diffusive problem (Alavyoon 1994) was used for the calculations. The numerical scheme is second-order accurate in space and first-order in time. The diffusion terms are calculated implicitly whereas the convection terms are taken explicitly. This leads to a stability restriction on the time step which becomes severe for high Rayleigh numbers. The variables solved for are stream function and temperature. A description of the original code can be found in Alavyoon (1994).

A uniform grid of 25 interior points in y and 75 in x was used for the cases presented. These calculations were made with the aspect ratio $A = 5$. Since the largest relevant time scale seems to be that of diffusion in the x-direction, which takes place on a dimensionless time scale of $t \sim A^2$, we would expect that initial transients have died out when $t \gg 25$. To be on the safe side, calculations were continued until $t = 300$.

Also, after the first submission of this paper, the authors gained access to a commercial flow prediction code, CFDS-FLOW3D†, which we have used in the Appendix to simulate a case with high Ra, moderate Pr, and $A = 1$. For this case a non-uniform 40 by 40 grid was used to resolve the boundary layers. A scheme which is second order in space and first order in time was employed.

5. Results

In the following, some analytical results are given, mainly in the form of $S(Ra;\alpha)$ curves. Five different values of the heating parameter γ have been considered and are presented as five different cases. For one special case ($\gamma = 225°, \alpha = 75°, Ra = 3000$) numerical results are also given.

5.1. *Case with equal heat fluxes, topmost side heated:* $\gamma = 45°$

With $\gamma = 45°$, one has $\lambda_1 = \lambda_2 = 1/\sqrt{2}$ from the definition (2.9*a*, *b*) and consequently no secular heating. With α between 0 and 90° the heated side is above the cooled side. For $\alpha = 90°$ there will be no convection, owing to hydrostatic stability, so one can expect a rather undramatic scenario as the box is laid down.

Figure 6 shows how the stratification varies with the Rayleigh number for different angles of inclination. There is only a single, positive, solution for S. For $\alpha = 0$, the non-dimensional stratification goes to zero for high Rayleigh numbers, in agreement with the results of Bark *et al.* (1992). If the enclosure is tilted however, the stratification instead approaches constant values which depend on the angle of inclination.

The situation for α close to 90° is that, for high Rayleigh numbers, the stratification, as we defined it, carries most of the heat flux whereas for low Rayleigh numbers the heat flux is mainly contained in the function f.

† Trademark of AEA Technology, CFDS, 8.19 Harwell, Didcot, Oxfordshire OX11 0RA, UK.

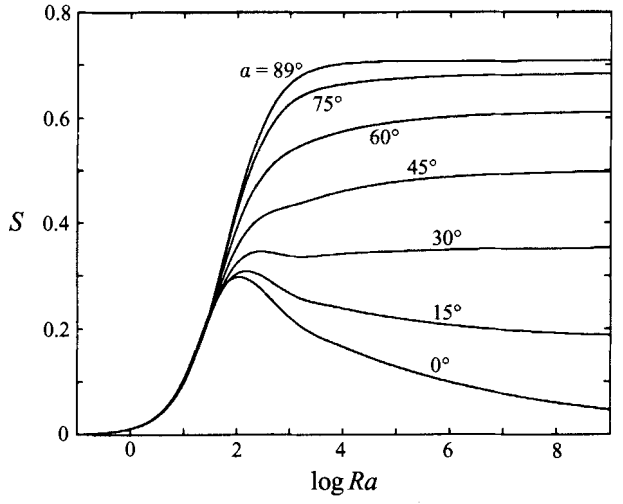

FIGURE 6. Stratification as function of Rayleigh number; $\gamma = 45°$.

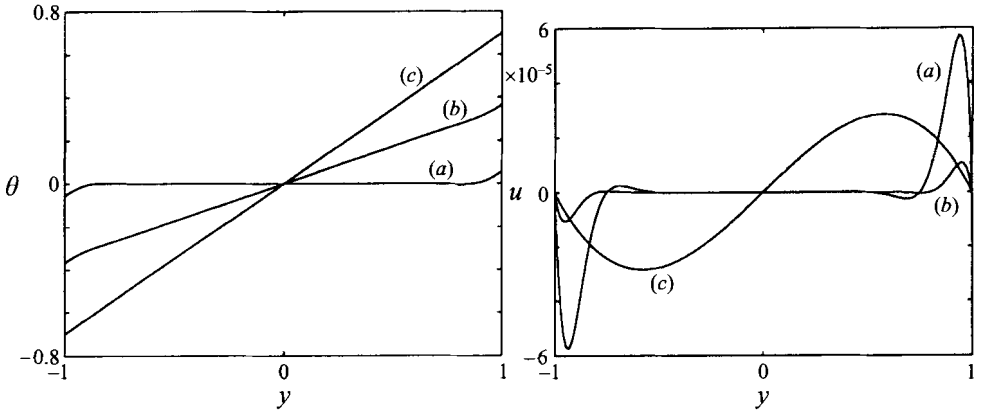

FIGURE 7. Some temperature and velocity profiles. (*a*) $Ra = 10^6, \alpha = 0$; (*b*) $Ra = 10^6, \alpha = 45°$; (*c*) $Ra = 10, \alpha = 45°$. For all cases $\gamma = 45°$.

Temperature and velocity profiles for three selected cases are shown in figure 7. For $\alpha = 0$, $Ra = 10^6$ both the temperature and the velocity profile have boundary layers. The thickness of the temperature boundary layer is the same as that of the velocity boundary layer, as is usually the case in a stratified environment. For the second case, the box has been inclined to $\alpha = 45°$, with Ra fixed at 10^6. The corresponding temperature profile reveals that the stratification serves to conduct a significant part of the heat directly from plate to plate. There are still boundary layers near the walls indicating that transport by convection is also important. For the third case we keep α at 45° and change Ra to 10. This gives a linear temperature profile, indicating that heat/mass transport occurs mainly by conduction. This fact is seemingly contradicted by the fact that the velocity u is *higher* than for the previous cases; but when u is multiplied by $Ra\,S\cos\alpha$ to form the convection term in the temperature equation (3.5), that term becomes negligible.

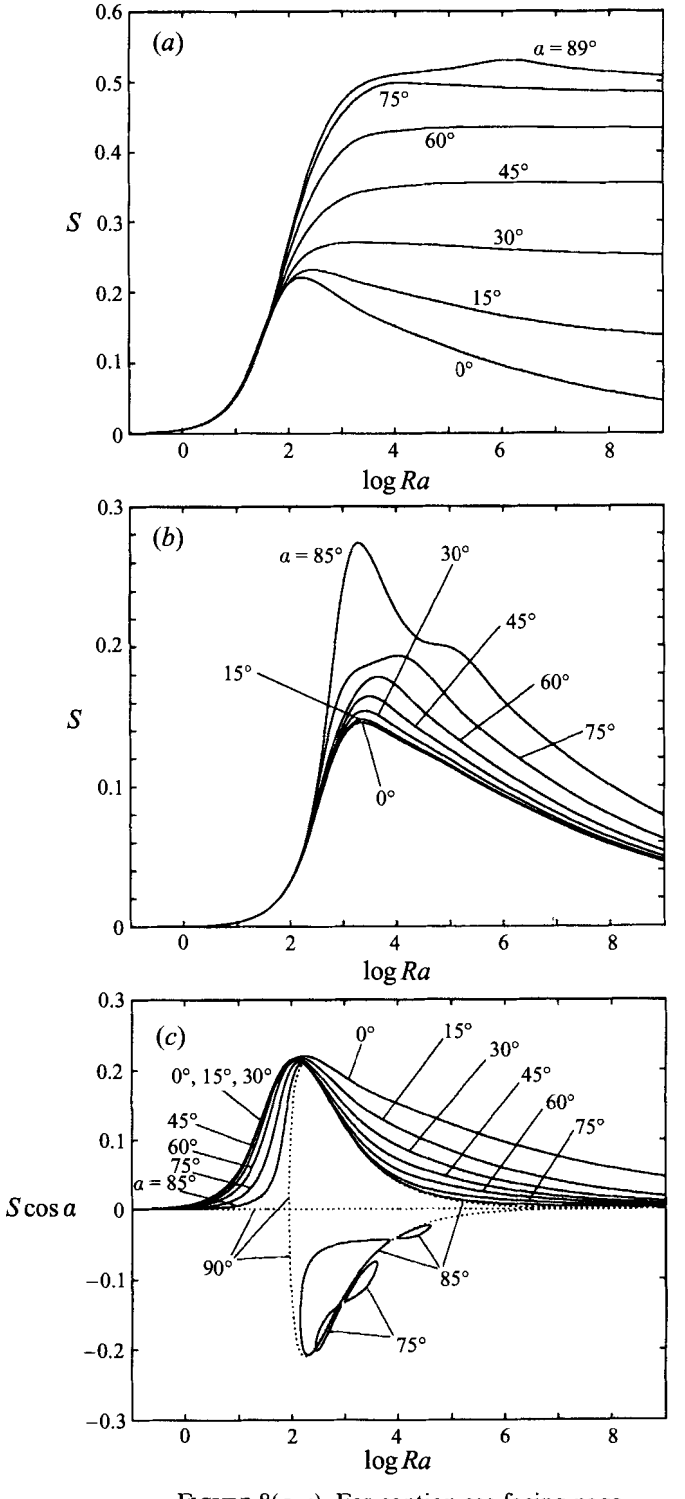

FIGURE 8(*a–c*). For caption see facing page.

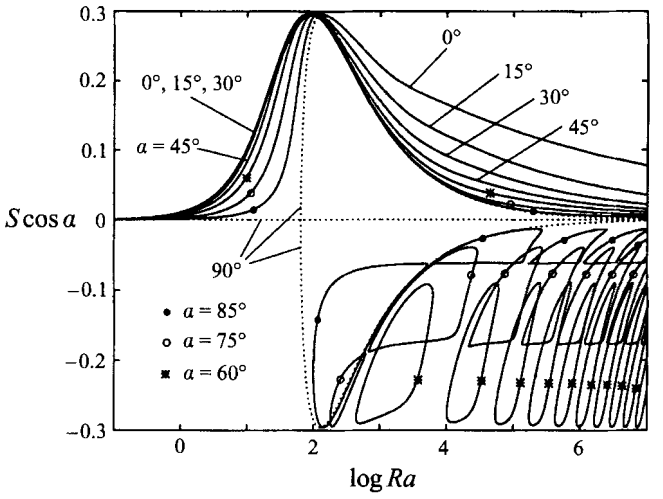

FIGURE 8. Stratification as function of Rayleigh number: (*a*) $\gamma = 90°$, (*b*) $\gamma = 135°$, (*c*) $\gamma = 180°$, (*d*) $\gamma = 225°$.

5.2. *Cases with secular heating:* $\gamma = 90°$, $\gamma = 135°$, *and* $\gamma = 180°$

We now change the type of forcing by changing the parameter γ.

The case $\gamma = 90°$ has heating from above with the lower boundary non-conducting. The resulting stratification, shown in figure 8 (*a*), looks similar to that of the $\gamma = 45°$ case although it tends to be somewhat weaker. Also, there is a small hump on the $\alpha = 89°$ curve which was not there before. Owing to the symmetry (3.37) the solution for S is also valid for the case of cooling from below.

The case $\gamma = 135°$ has equal heating from both sides. Figure 8(*b*) shows the resulting $S(Ra)$ curves. Here, the stratification no longer approaches α-dependent constant values for large Ra but instead goes to zero for all angles of inclination. Also, the hump has evolved into a singularity at $\alpha = 90°$. However, a closer look at data near the singular point reveals that all physical quantities remain finite as $\alpha \to 90°$. The quantity β approaches zero due to the factor $\cos^2\alpha$ whereby $F_0 \to y$ so that the contribution of F_0 to θ cancels out the stratification term $S\,y\sin\alpha$. The temperature gradient in the x-direction, which is $S\cos\alpha$, also remains finite and in fact goes to zero as $\alpha \to 90°$. In the figure, the $\alpha = 89°$ curve has been replaced with one for $\alpha = 85°$ so as not to get too close to the singularity.

The case $\gamma = 180°$ has the lowermost side heated and the topmost side non-conducting. Just as for the previous case, S becomes weakly singular as $\alpha \to 90°$ and, just as for that case, all physical quantities remain finite. Here the temperature gradient in the x-direction becomes finite and non-zero which is why we have chosen to plot that quantity, $S\cos\alpha$ instead of S. As can be seen from figure 8(*c*), there is a parameter region where negative solutions exist for S. The negative solutions are related to the bifurcation occurring for the horizontal case and they appear when the box is close to horizontal position. However, as soon as the box is not completely horizontal, there is a preferred flow direction - that which is associated with a positive S. The figure shows that, as the box is moved away from $\alpha = 90°$, the negative solution branch becomes a twisted loop with no direct connection to the positive solution branch, the latter now being a smooth curve (plots with increased resolution indicate that there *is* indeed a twisted loop rather than two disconnected loops). This structure of the

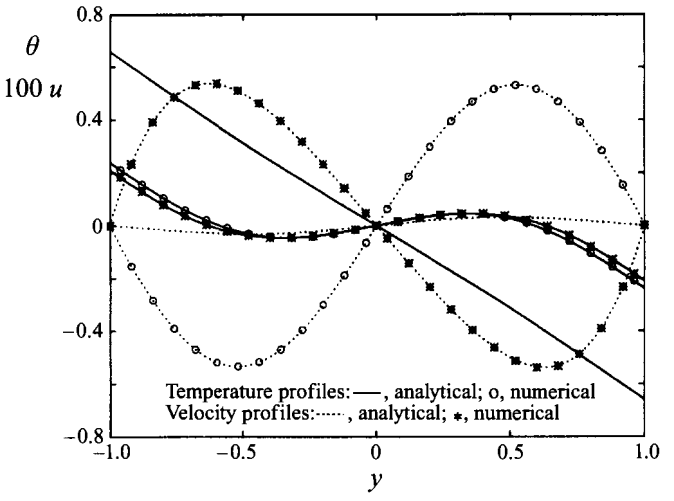

FIGURE 9. Temperature and velocity profiles for $\gamma = 225°, \alpha = 75°, Ra = 3000$ (3 solutions).

branches seems to confirm the intuitive notion that a negative stratification cannot be reached naturally from rest. The negative solutions were graphically found to disappear at $\alpha = 66° \pm 0.5°$. As this value is approached, the twisted loop eventually shrinks to a point, located slightly below the centre of the $\alpha = 75°$ loop. For a porous medium with prescribed wall temperatures, Riley & Winters (1990) give a fuller description of a similar bifurcation structure. In the terminology used by those authors, what we observe is a pitchfork bifurcation at $\alpha = 90°$ which, as α is decreased, unfolds to form an isola (a closed loop). As α is decreased further the isola eventually vanishes at a critical angle $\alpha \approx 66°$ which, together with Ra, defines an isola formation point. Naturally, the complete bifurcation diagram cannot be found from a simple steady-state ansatz like ours, but would require further analysis – for instance using the methods of Riley & Winters (1990).

5.3. *Case with equal heat fluxes, topmost side cooled:* $\gamma = 225°$

This case has heating at the bottom and cooling on top. Just as for $\gamma = 45°$ the fluxes are equal so that no secular heating occurs. Figure 8(*d*) reveals a structure of the solution branches which is even more complicated than that of the $\gamma = 180°$ case. To maintain a reasonable plot resolution, the plot range for Ra has been made two decades smaller than that of the previous figures. Symbols have been put in to help distinguish the different curves.

The twisted loop structures are still present. They are here even larger than for the previous, $\gamma = 180°$, case. For high Rayleigh numbers, there is also a large number of disconnected loops which become increasingly thin and more densely packed as Ra is increased. This packing of loops causes the number of solutions to increase with Ra. In the figure there are at the most seven solutions and if the Rayleigh number is increased further even more solutions appear.

Figure 9 shows a comparison between analytically predicted and numerically simulated temperature and velocity profiles for the case $\alpha = 75°, Ra = 3000$ which gives one positive solution and two negative solutions, the latter being located on the right part of the twisted loop for $\alpha = 75°$. The numerical data were taken at mid-height. For the temperature profiles the mean value was subtracted – owing to end effects this mean value was not exactly zero.

The positive solution ($S = 0.0870$) has a natural flow direction, meaning a positive correlation between u and θ in the cross-section. This solution could easily be reproduced in a numerical simulation starting from rest.

The second solution is negative ($S = -0.0891$), giving almost the same temperature profile and a velocity profile which has about the same amplitude but the opposite sign. Since both S and u change sign, the convection term $Ra\,S\,u\cos\alpha$ becomes almost the same as for the first solution. To obtain this solution from rest, the box was first pre-stratified at $\alpha = 105°$ until a steady state was reached. Then, the tilting angle α was instantaneously reduced to 75° and heating was continued until a new steady state had been reached. This method originates from Sen *et al.* (1987) who used it to numerically simulate steady states with unnatural stratification in a porous medium (those authors used the adjective 'antinatural' to describe such a stratification). Since stratification evolves on a very large timescale, we believe that it is possible to use the same method to experimentally find steady states with unnatural stratification. The tilting should be performed gently, avoiding strong mixing, but presumably there is no need to do it very quickly. It should be noted that a work by Lavine (1993) states that unnatural stratification is unstable (to zero-wavenumber perturbations) under certain circumstances which are all fulfilled by the present case. However, in that work no account whatsoever was taken of end-region boundary conditions. As a consequence, Lavine's analysis violates both (3.7) and (3.9), and is not applicable here.

The third solution ($S = -0.175$) has a very weak flow in the unnatural direction and a temperature profile which is almost a straight line, indicating pure conduction. This solution could not be reproduced in the numerical simulations however – most likely it is unstable.

Simulations with Rayleigh numbers within the left part of the twisted loop have also been made. Those simulations gave similar results except that on this side of the twist, the conduction branch is the one with the smallest absolute value of S.

6. Validity restrictions

As we have seen, the stratification parameter S does not depend on the aspect ratio A, but only on Ra, α, and γ, none of which contains the box length in the x-direction, H. Thus, the x-derivative of the temperature is independent of the length of the box in the x-direction. This means that, as H is increased, we will eventually reach a point where the temperature differences near the ends become so large that the constant-property assumption and/or the Boussinesq assumption breaks down. If we allow a maximum temperature difference of $(\Delta T)_{max}$ the following condition must be fulfilled:

$$H < \frac{(\Delta T)_{max}}{A_T S \cos\alpha}, \tag{6.1}$$

and similarly for the mass transfer case. This condition appears not to have been noted in previous work with constant-flux boundary conditions, but is nevertheless of importance. For instance, because of this condition we cannot use the present solution to treat double-glazed windows under normal circumstances. The solution of the mathematical problem would still be correct, but the problem itself would not model reality very well.

Another restriction is that the aspect ratio must be large compared to the boundary

layer thickness:

$$A \gg \min(\beta^{-1}, 1). \tag{6.2}$$

Also, because of our two-dimensional analysis, the dimension of the enclosure perpendicular to the paper in figure 1 must be much larger than the plate distance h.

There are two different nonlinear terms in the original equations, each of which may cause instability for high Rayleigh numbers. We consider first the nonlinear term in the momentum equation and estimate, from our different explicit solutions, a Reynolds number based on velocity amplitude and profile thickness:

$$Re \sim \begin{cases} O\left(Ra^{1/9}/Pr\right), & \text{for } \alpha = 0,\ \gamma \text{ arbitrary} \\ O\left(1/Pr\right), & \text{for } \sin\alpha, \cos\alpha \sim O(1), \lambda_1 + \lambda_2 > 0 \\ O\left(Ra(Ra - Ra_{cr})^{1/2}/Pr\right), & \text{for } \alpha = 90°, \lambda_1 + \lambda_2 < 0. \end{cases} \tag{6.3}$$

Except for in the Bénard limit (or near it), the Reynolds number grows slowly or (this may seem surprising) not at all with Ra. It seems that the term is a potential source of breakdown of our unicell solutions only for small Pr and/or bottom-heated enclosures.

The nonlinear term in the temperature equation, on the other hand, is generally important for high Rayleigh numbers (except when the enclosure is almost horizontal and top-heated). Near the Bénard limit, we have already seen how it causes a gravitational instability and it would not be surprising if it causes further instabilities.

For vertical or stably inclined cases, a somewhat brutal extension of the results of Hart (1971) indicates breakdown of the unicells around $Ra \sim 10^5$. However, a numerical simulation at $Ra = 1.4 \times 10^6$ (see Appendix) did not show any tendency for breakdown, which may indicate that the critical Rayleigh number is significantly higher – although it should be noted that the simulation was made in two dimensions and therefore excludes any three-dimensional instabilities.

Further analysis is definitely necessary to determine critical Rayleigh numbers and instability mechanisms.

7. Some limiting cases

For some parameter regions we have derived approximate solutions in explicit form. These can be used to obtain results quickly and may also give some additional insight.

7.1. *High Rayleigh number limit*

Guided by the numerical solution of equation (3.14) and by the result of Bark *et al.* (1992) we assume that a large Ra also implies a large β, and simplify (3.14) accordingly before expanding in Ra. The method may not be formally correct, but nevertheless leads to expansions which agree well with the numerical solution of (3.14). For large β

$$(I_1, I_2, I_3) \to \frac{1}{2\beta^4}\left(\frac{1}{4\beta},\ 1 - \frac{1}{\beta},\ \frac{1}{4\beta} - \frac{1}{2\beta^2} + \frac{3}{8\beta^3}\right). \tag{7.1}$$

The corresponding cross-sectional profiles have boundary layer character with exponential functions multiplying sines and cosines. An example is shown in the Appendix. For a vertical enclosure ($\alpha = 0$) we get the following solution for S:

$$S \approx 0.463 Ra^{-1/9} - 0.353\,(1 - \sin 2\gamma)\, Ra^{-3/9} + O(Ra^{-5/9}) \tag{7.2}$$

which, except for cosmetic details, is identical to the result of Bark *et al.* (1992). Note here that the lowest-order term is independent of the heating parameter γ. For cases without secular heating $\sin 2\gamma = 1$ and the correction terms vanish so that the only error comes from expanding I_1 for large β. The errors in the I_1, I_2, I_3 expansions all decay exponentially with $\beta \approx 0.583 Ra^{2/9}$ and thus quickly become negligible as Ra is increased.

For the more general case of a non-zero α it is difficult to obtain expansions since different parameter regions must be treated differently. For inclination with the heaviest side down ($\sin\alpha(\lambda_1 + \lambda_2) > 0$) we found the following expansion:

$$S = S_0 + \frac{Ra^{-1/4}}{S_0}\left(\frac{S_0 \cos^2\alpha}{4}\right)^{-1/4}\left\{\tfrac{1}{8} + \tfrac{5}{4}S_0^2 \sin^2\alpha - \tfrac{3}{2}S_0^2\right\} + O(Ra^{-1/2}) \tag{7.3}$$

where

$$S_0 = \frac{\lambda_1 + \lambda_2}{2}\sin\alpha.$$

S is here found to approach the constant value S_0 as $Ra \to \infty$. In parameter regions where the second term in (7.3) becomes larger than the first term, the expansion ceases to be valid. The matter of finding expansions for different parameter regions has not been pursued further.

7.2. *Low Rayleigh number limit*

For low Ra we can neglect the convection contribution in (3.5). Doing so we get the following solutions:

$$F_O = y, \quad U_O = \frac{y - y^3}{6}, \quad F_E = \frac{y^2}{2} - \frac{1}{6}, \quad U_E = \frac{6y^2 - 5y^4 - 1}{120}. \tag{7.4a–d}$$

In this limit, both the velocity field and the stratification that it causes are passive and do not influence the cross-sectional temperature profile. The integrals in (3.14) become

$$(I_1, I_2, I_3) = \left(\frac{2}{45}, \frac{2}{45}, \frac{2}{1575}\right) \tag{7.5}$$

which leads to the following unique solution for S:

$$S = \frac{Ra}{70}\,\frac{(\lambda_2 - \lambda_1)^2 + 35(\lambda_1 + \lambda_2)^2}{90 + Ra(\lambda_1 + \lambda_2)\sin\alpha}. \tag{7.6}$$

For very low Rayleigh numbers, S grows linearly with Ra and is independent of α. For higher Ra there is also an α-dependence and, for $(\lambda_1 + \lambda_2)$ negative, a singular point where (7.6) breaks down. For the horizontal case, this breakdown occurs exactly at the previously calculated bifurcation point.

Another conclusion to draw from (7.6) is that, for low Rayleigh numbers, an even forcing $(\lambda_2 - \lambda_1)$ is much less effective than an odd forcing $(\lambda_1 + \lambda_2)$ in setting up a stratification. This is in contrast to the limit $Ra \to \infty, \alpha = 0$, for which the lowest order term in (7.2) has odd and even forcing of equal weight. Note that $1 = \lambda_1^2 + \lambda_2^2 \propto (\lambda_2 - \lambda_1)^2 + (\lambda_1 + \lambda_2)^2$.

7.3. *Validity ranges for the approximate solutions*

Figure 10 shows the validity ranges for the above expansions when $\gamma = 45°$. Because the range in α has been extended to $-90° < \alpha < 90°$, the figure also covers the case $\gamma = 225°$, as can be seen from the symmetry (3.35).

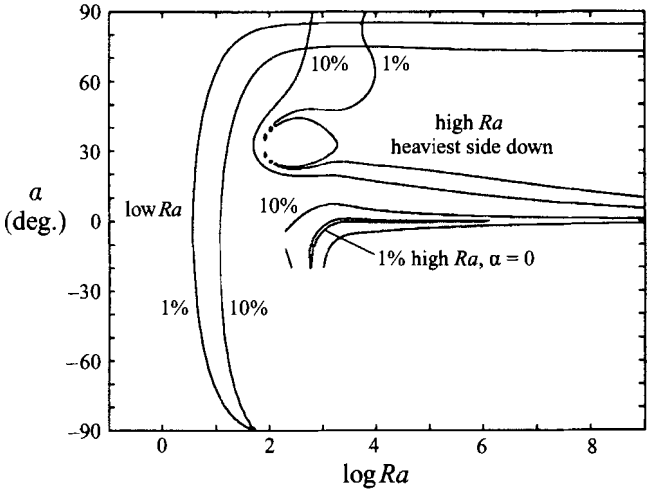

FIGURE 10. Validity regions of high- and low-Ra solutions, $\gamma = 45°$. The figure shows contours of the relative error when the approximate solutions are compared with a numerical solution of the stratification equation.

The $\alpha = 0$-high Ra model is seen to be valid for Ra greater than about 1000. It also happens to agree in a thin region of complex geometry not shown in the figure.

The high-Ra model for non-zero α has a similar Rayleigh number restriction. Also, α should not be too small for the model to be valid.

The validity of the low-Ra solution depends on the smallness of $Ra\,S\cos\alpha$ and we see from the figure that the model works even for high Ra in the special case when the box is almost horizontal with the heaviest side down.

8. Summary and conclusions

Buoyancy-driven flows in a rectangular space having an arbitrary inclination with respect to gravity were studied analytically. The flows studied are driven by constant, but not necessarily equal, fluxes applied along two opposing walls.

Solutions valid for large times, sufficiently far from the end regions, were sought, assuming a uni-directional flow and a linear temperature (concentration) variation in the flow direction.

In the first step, cross-sectional temperature and velocity profiles were obtained as functions of a stratification constant S, at this point unknown. To close the problem, the energy flux condition was applied, giving a nonlinear algebraic equation to solve for S. The equation for S was solved numerically for a large set of different parameters – except for the special case of horizontal orientation for which a simple explicit solution was found. Important parameters in the system are the heating condition parameter γ, the inclination angle α, and the Rayleigh number Ra.

When the system is mainly top- or side-heated, the solution for S is uniquely determined. On the other hand, when it is mainly bottom-heated, multiple solutions appear when Ra is high enough and the orientation is close enough to horizontal. The additional solutions all have negative values of S which means an unnatural (top-heavy) stratification.

A few selected cases were also solved numerically. First, the unsteady creeping flow equations ($Pr \to \infty$) were solved for a case with multiple solutions in a box with the

aspect ratio $A = 5$. Both natural and, with some tricks, unnatural stratifications could be obtained. Very good agreement between analytical and numerical results shows that solutions of the type sought can be approached and gives a strong indication that the analytical expressions we have found are correct. Secondly, the full unsteady equations were solved for a case with high Ra and moderate Pr, and again showed very good agreement, also with an analytical end-region solution which was derived for the case of equal fluxes and stable inclination.

Simple explicit forms of the analytical solution were derived for the two asymptotic limits of high and low Rayleigh numbers. Their regions of validity were determined by a comparison with the exact solution.

In closing the present study, it should be noted that even though we have found a family of exact solutions to the governing nonlinear partial differential equations, previous experience with similar flows, see for instance Hart (1971), suggests that for sufficiently large values of Ra these solutions will become unstable. Also, it is evident that in the multiple solution region some of the solutions are not stable. A rigorous investigation of this matter goes beyond the scope of the present study and is therefore left for a future project.

We wish to thank Professor Fritz Bark at the department of Mechanics, KTH, for suggesting the original version of this problem and Dr Farid Alavyoon at Vattenfall Utveckling AB, Älvkarleby, Sweden, for letting us use his computer code. Also, the financial support from the Swedish National Board for Industrial and Technical Development (NUTEK) and the Erik Petersohn memorial foundation is gratefully acknowledged.

Appendix. On the end regions

Near the ends $x = \pm A$, the inner-region solutions are not valid. When deriving the inner-region solutions we have assumed that the details of the end regions are not felt at a long distance so that all we need to know from the end regions is the total flux of internal energy and mass. Since this information could be derived directly from the boundary conditions, there has been no need to solve the end regions and match them to the interior. This is a major difference from the case with prescribed wall temperature, in which the boundary conditions alone are not enough to obtain the energy flux. From the viewpoint of less idealized boundary conditions, for instance of the type $\partial\theta/\partial y = Nu(\theta - \theta_0)$, the constant-flux case emerges as a particularly simple special case, whereas the much more researched constant-temperature case may even be thought of as a particularly difficult special case.

For the vertical case, Bark *et al.* (1992) write down some equations for solving the end regions and conclude, from an analogy with the so-called Stewartson layers found in rotating flows, that the end regions, for high Ra and $\alpha = 0$, are nonlinear and have a thickness which scales with $h/Ra^{1/9}$.

For high Rayleigh numbers and a tilt angle α which is not very close to 0 or 90°, the end-region problem, oddly enough, becomes very simple. This is due to the fact that the stratification, which is in the direction of gravity, will have a component along the endwalls. Owing to this, the endwalls will be governed by essentially the same equations as the sidewalls! The situation is particularly simple for the case of equal fluxes, in which there is no flow in the interior. It is here a straightforward matter to derive the following boundary-layer solution, valid everywhere, except in

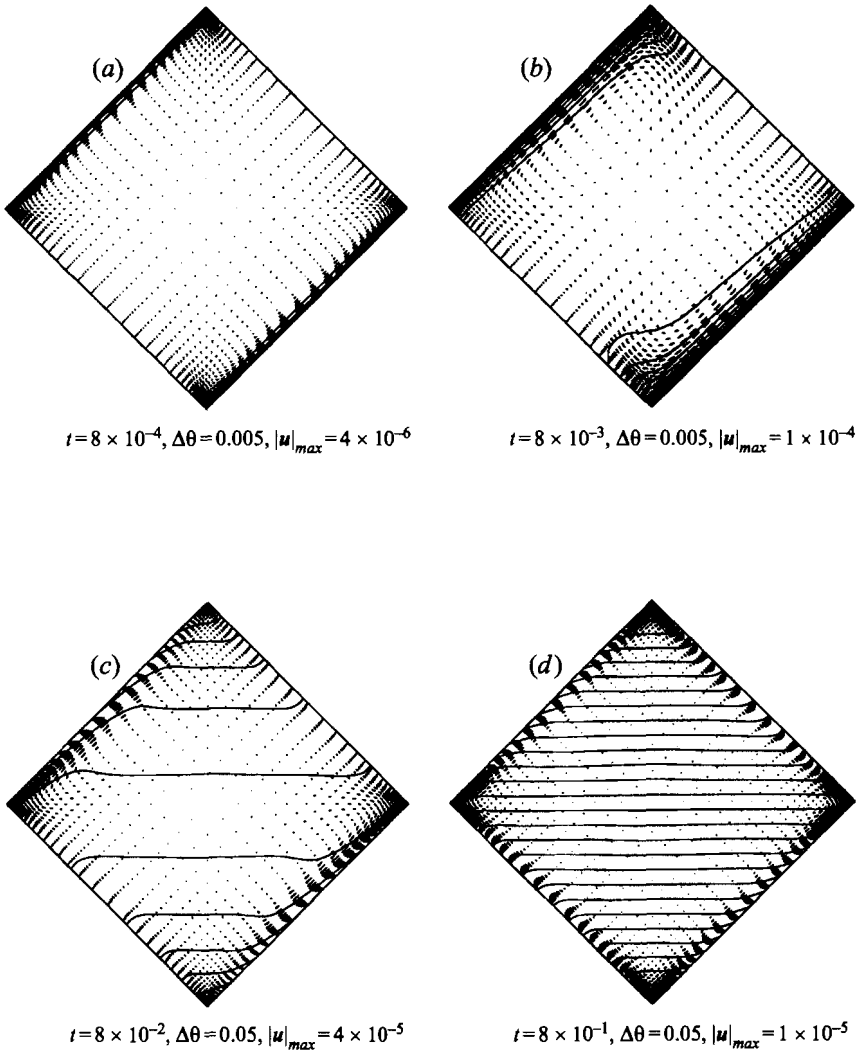

FIGURE 11. Numerical simulation with $Ra = 1.4\times10^6, \alpha = \gamma = 45°, A = 1, Pr = 7$. (*a*) Boundary layers start to grow. The flow is parallel with only a weak passive convection. (*b*) The boundary-layer growth has become inhibited by convection. Velocities are higher and the flow no longer parallel. (*c*) A stratification develops in the interior. This damps the flow and compresses the boundary layers. (*d*) A steady state with a parallel flow and a linear stratification has been reached.

the four corners:

$$\theta = S(x\cos\alpha + y\sin\alpha) + \frac{S\cos\alpha}{\beta_E}\left\{e^{-\beta_E(A+x)}\cos\beta_E(A+x) - e^{-\beta_E(A-x)}\cos\beta_E(A-x)\right\}$$
$$+\frac{2^{-1/2} - S\sin\alpha}{\beta}\left\{e^{-\beta(1-y)}\cos\beta(1-y) - e^{-\beta(1+y)}\cos\beta(1+y)\right\}, \tag{A 1}$$

$$\boldsymbol{u} = \frac{S\cos\alpha\sin\alpha}{2\beta_E^3}\left\{e^{-\beta_E(A+x)}\sin\beta_E(A+x) - e^{-\beta_E(A-x)}\sin\beta_E(A-x)\right\}\boldsymbol{e}_y$$
$$+\frac{\cos\alpha(2^{-1/2} - S\sin\alpha)}{2\beta^3}\left\{e^{-\beta(1-y)}\sin\beta(1-y) - e^{-\beta(1+y)}\sin\beta(1+y)\right\}\boldsymbol{e}_x, \tag{A 2}$$

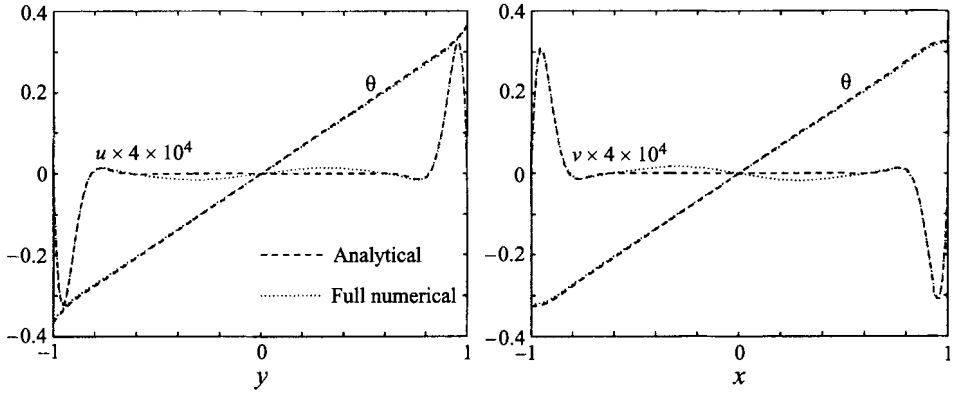

FIGURE 12. Temperature and velocity profiles in two perpendicular cross-sections through figure 11(*d*) compared with the analytical predictions.

where

$$\beta_E = \left(\frac{RaS\sin^2\alpha}{4}\right)^{1/4}, \qquad \beta = \left(\frac{RaS\cos^2\alpha}{4}\right)^{1/4}. \tag{A 3}$$

For inclination with the heaviest side down, we can obtain S explicitly from (7.3).

Finally, to validate this solution and at the same time exemplify that the parallel flow solutions that we have studied in this paper are realizable even for moderate A and Pr, we have made a full numerical simulation for the case $A = 1, Pr = 7, Ra = 1.4 \times 10^6, \gamma = 45°, \alpha = 45°$. This has been done using the commercial flow prediction code CFDS-FLOW3D. The unsteady problem was solved from rest until a dimensionless time of $t = 0.8$. Figure 11(*a–d*) shows how the flow develops with time and eventually reaches a steady state with linear stratification and boundary layers with parallel flow. Figure 12, finally, shows a comparison between the analytical solution (A 1) and the numerical result for $t = 0.8$. A difference can only be seen in the velocity profiles near the middle. Presumably, even that small difference would vanish as $t \to \infty$.

REFERENCES

ALAVYOON, F. 1994 Double diffusive natural convection in a slender enclosure - cooperative solutal and thermal buoyancy forces. In *Proc. 3rd JSME-KSME Fluid Engng. Conf.*

BARK, F. H., ALAVYOON, F. & DAHLKILD, A. 1992 On unsteady free convection in vertical slots due to prescribed fluxes of heat or mass at the vertical walls. *J. Fluid Mech.* **235**, 665.

BATCHELOR, G. K. 1954 Heat transfer by free convection across a closed cavity between vertical boundaries at different temperatures. *Q. J. Appl. Maths* **12**, 209.

BEJAN, A. 1979 Note on Gill's solution for free convection in a vertical enclosure. *J. Fluid Mech.* **71**, 729.

BRENT, R. P. 1973 *Algorithms for Minimization without Derivatives.* Prentice-Hall.

BUSSE, F. H. 1978 Nonlinear properties of convection. *Rep. Prog. Phys.* **41**, 1929.

DAVIS, S. H. 1967 Convection in a box: linear theory. *J. Fluid Mech.* **30**, 465.

DRAZIN, P. G. & REID, W. H. 1981 *Hydrodynamic Stability.* Cambridge University Press.

ELDER, J. W. 1965 Laminar free convection in a vertical slot. *J. Fluid Mech.* **23**, 77.

GILL, A. E. 1966 The boundary-layer regime for convection in a rectangular cavity. *J. Fluid Mech.* **26**, 515.

HART, J. E. 1971 Stability of the flow in a differentially heated inclined box. *J. Fluid Mech.* **47**, 547.

KIMURA, S. & BEJAN, A. 1984 The boundary layer natural convection regime in a rectangular cavity with uniform heat flux from the side. *Trans. ASME* C: *J. Heat Transfer* **106**, 98.

KIMURA, S., VYNNYCKY, M. & ALAVYOON, F. 1995 Unicellular natural circulation in a shallow horizontal porous layer heated from below by a constant flux. *J. Fluid Mech.* **294**, 231.

LAVINE, A. 1993 On the linear stability of mixed and free convection between inclined parallel plates with fixed heat flux boundary conditions. *Intl J. Heat Mass Transfer* **36**, 1373.

NEWMAN, J. S. 1991 *Electrochemical Systems*, 2nd edn. Prentice-Hall.

PATTERSON, J. & IMBERGER, J. 1980 Unsteady natural convection in a rectangular cavity. *J. Fluid Mech.* **100**, 65.

PRANDTL, L. 1952 Mountain and valley winds in stratified air. In *Essentials of Fluid Dynamics*, Chap V:16. Blackie & Son.

PRESS, W., FLANNERY, B., TEUKOLSKY, S. & VETTERLING, W. 1986 *Numerical Recipes*. Cambridge University Press.

RILEY, D. S. & WINTERS K. H. 1990 Natural convection in a tilted two-dimensional porous cavity. *J. Fluid Mech.* **215**, 309.

SCHLADOW, S. G. 1990 Oscillatory motion in a side-heated cavity. *J. Fluid Mech.* **213**, 589.

SEN, M., VASSEUR, P. & ROBILLARD, L. 1987 Multiple steady states for unicellular natural convection in an inclined porous layer. *Intl J. Heat Mass Transfer* **30**, 2097.

SPARROW, E., GOLDSTEIN, R. & JONSSON, V. 1963 Thermal instability in a horizontal fluid layer: effect of boundary conditions and non-linear temperature profile. *J. Fluid Mech.* **18**, 513.

STELLA F., GUJ, G. & LEONARDI, E. 1993 The Rayleigh–Bénard problem in intermediate bounded domains. *J. Fluid Mech.* **254**, 375.